ChemistrySelect

Research Article
doi.org/10.1002/slct.202500588

Chemistry Europe
European Chemical Societies Publishing

www.chemistryselect.org

Investigating the Antitumor Efficacy of NL2 Peptide-Conjugated Silica Nanoparticles Loaded with NANOG Decoy Oligodeoxynucleotides for Targeted Delivery into Breast Cancer Cells

Roghayeh Ghorbani,[a, b, c] Mahmoud Gharbavi,[d, e] Behrooz Johari,*[f] Zahra Bigdelou,[c] Zeinab Pourmansouri,[g] Niloofar Asadi,[c] Nazli Aghapur,[c] Benyamin Keshavarz,[c] and Hamid Madanch*[h, i, j]

NANOG transcription factor, a molecule associated with cancer cell resistance, was targeted using decoy oligodeoxynucleotides (ODNs) loaded nanoparticles. We designed decoy ODN to mimic a human gene promoter, aiming to disrupt the function of NANOG. Silica (SiO_2) nanoparticles were coated with polydopamine (PDOPA) and loaded with decoy ODNs. These nanoparticles were then functionalized with a targeting agent, the NL2 peptide, to achieve specific binding to HER2-positive cells. Following this, their physicochemical properties were characterized using Fourier-transform infrared spectroscopy (FT-IR), dynamic light scattering (DLS), scanning electron microscopy (SEM), UV–visible spectroscopy (UV–vis), and drug release assays. The effectiveness of these nanoparticles was then tested on SKBR3 (HER2 positive) and MDA-MB-468 (HER2 negative) breast cancer cells. The results were encouraging the nanocomposites were successfully absorbed by the cancer cells. SiO_2@PDOPA/DEC-NL2 significantly inhibits cell growth and increased cell death (apoptosis). These findings suggest that the synthesized nanosystem targeting the HER2 receptor can potentially suppress the cancerous properties of SKBR3 cells in comparison with MDA-MB-468 cells. In conclusion, this study presents a promising approach for targeted drug delivery in breast cancer treatment. The developed nanoparticles loaded with NANOG decoy ODNs effectively targeted HER2-positive cancer cells and demonstrated significant anticancer properties.

1. Introduction

In recent years, breast cancer has accounted for around 2.3 million new cases globally among both genders.[1] By 2040, the number of new cases of breast cancer is predicted to increase by more than 40%, and the number of deaths growing by over 50% (from 685,000 in 2020 to 1 million in 2040).[2]

Cancer can be caused by many genetic and epigenetic changes.[3] Transcription factors (TFs) are commonly deregulated in cancer pathogenesis and can represent a unique class of drug targets.[4] NANOG transcription factor expression is very low in human tissues postnatally, and its overexpression can lead to carcinogenesis. The aberrant expression of NANOG confers properties similar to stem cells to cancer cells and increases the growth and proliferation of tumor cells and subsequently their metastasis and recurrence.[5,6] Furthermore, the high expression level of this transcription factor was shown to be correlated with low survival of breast cancer patients.[7,8] Studies found

[a] R. Ghorbani
Cellular and Molecular Research Center, Cellular and Molecular Medicine Research Institute, Urmia University of Medical Sciences, Urmia, Iran

[b] R. Ghorbani
Department of Applied Cell Sciences, Faculty of Medicine, Urmia University of Medical Sciences, Urmia, Iran

[c] R. Ghorbani, Z. Bigdelou, N. Asadi, N. Aghapur, B. Keshavarz
Department of Medical Biotechnology, School of Medicine, Zanjan University of Medical Sciences, Zanjan, Iran

[d] M. Gharbavi
Nanotechnology Research Center, Medical Basic Sciences Research Institute, Ahvaz Jundishapur University of Medical Sciences, Ahvaz, Iran

[e] M. Gharbavi
Pain Research Center, Ahvaz Jundishapur University of Medical Sciences, Ahvaz, Iran

[f] B. Johari
Zanjan Pharmaceutical Nanotechnology Research Center (ZPNRC), Zanjan University of Medical Sciences, Zanjan, Iran
E-mail: Dr.johari@zums.ac.ir

[g] Z. Pourmansouri
Department of Pharmacology, School of Medicine, Zanjan University of Medical Sciences, Zanjan, Iran

[h] H. Madanch
Nervous System Stem Cells Research Center, Semnan University of Medical Sciences, Semnan, Iran
E-mail: hamidmadanchi@semums.ac.ir

[i] H. Madanch
Department of Medical Biotechnology, Faculty of Medicine, Semnan University of Medical Sciences, Semnan, Iran

[j] H. Madanch
Drug Design and Bioinformatics Unit, Biotechnology Research Center, Pasteur Institute of Iran, Tehran, Iran

that NANOG was highly expressed in breast SKBR3 cell lines.[9] Therefore, the NANOG transcription factor can be considered an important therapeutic target for this HER2-positive cancer.

Current treatment approaches for breast cancer are such as surgery, chemotherapy, radiation, and hormone therapy.[10–12] Radiotherapy and chemotherapy are satisfactory for the treatment of cancer in the early stages[13] but not for the advanced stages of cancer. Each of these treatment methods has its drawbacks. In the radiotherapy strategy, some tumor cells remain and cause tumor recurrence and metastasis.[14] In addition, chemotherapy is commonly associated with severe systemic toxicity and chemoresistance.[15] Along with chemotherapy and radiotherapy, endocrine and anti-HER2 therapies are also used, which can have severe side effects and cause resistance to these types of treatments in patients.[16] Therefore, safe and effective treatment strategies are urgently needed for cancer treatment. Decoy oligodeoxynucleotides (ODNs) as novel agents (based on nucleotide sequences) are used as a gene therapy method by blocking transcription factors.[17] Decoy oligodeoxynucleotides (ODNs) offer a groundbreaking strategy in gene therapy by disrupting transcription factor activity. These lab-engineered, double-stranded DNA molecules are crafted to imitate specific promoter or enhancer sequences in the genome. By attaching to transcription factors, decoy ODNs block these proteins from binding to their natural DNA targets, thereby influencing gene expression. This approach shows great potential for treating diseases linked to abnormal transcription factor activity, including cancer and inflammatory conditions.[18–20]

Nowadays, nonviral vectors are widely used for cancer gene therapy due to their lack of immunogenicity.[21] Core/shell nanocomposites and modified nanoparticles with biocompatible reagents are promising carriers for use in biomedical applications.[22] Silica nanoparticles (SiO_2NPs) have many remarkable and excellent properties, including mechanical stability and high permeability, great tolerance to chemicals, and a high surface-to-volume ratio.[23] To increase the biocompatibility and the dispersion ability of these nanoparticles in body fluids and reduce their burst drug-release behavior, their surface is usually modified using polymers such as polydopamine (PDOPA). Based on previous studies, L-DOPA (3,4-dihydroxyphenylalanine), a nonessential amino acid, exhibits good potential for developing organic/inorganic nanocomposites.[24] PDOPA was utilized as a surface polymer to enable the pH-responsive release of anticancer agents.[25,26] Under basic conditions, dopamine self-polymerizes to form a robust polydopamine coating that strongly adheres to the surfaces of NPs without any preliminary surface modification.[27,28]

Targeted drug delivery to the tumor site is a major problem in cancer treatment strategies, and their use in conventional methods is associated with poor biodistribution and limited effectiveness, as well as many side effects.[29] Many studies have investigated various biological ligands for the active targeting of nanoparticles.[30] These biological ligands are often specific for special receptors on the surface of target cells, and by binding to these receptors, they increase the cellular uptake of nanoparticles that may also contain a specific drug.[31] Tumor targeting peptides (TTPs) with 3–15 amino acids are one of the mentioned ligands. One of these peptides that target tumors is the NL2, which exhibits a strong affinity for HER2 receptors in breast cancer cells that overexpress them.[32]

In the present study, silica (SiO_2) nanoparticles were coated with polydopamine (PDOPA) and subsequently loaded with NANOG decoy ODNs (SiO_2@PDOPA/ODNs). These nanoparticles were then functionalized with a targeting agent, the NL2 peptide (SiO_2@PDOPA/ODNs-NL2), to achieve specific binding to HER2-positive cells. Following synthesis, the physicochemical properties of the nanocomposites were comprehensively characterized using various techniques, including FT-IR, DLS, SEM, UV–vis, and drug release assays. Subsequently, the anticancer efficacy of these nanocomposites was evaluated through the MTT and apoptosis assays for cytotoxicity and quantifying the cell death, respectively (Figure 1).

2. Materials and Methods

2.1. Reagents

Average-sized silica nanoparticles (15 nm) with ~99.9% pure chemicals were purchased from the US Nano Company. NHS (*N*-hydroxysuccinimide) and EDC [*n*-ethyl-n′-(3-dimethyl aminopropyl) carbodiimide hydrochloride] used in nanocomposite preparation were purchased from Merck (Darmstadt, Germany). L-DOPA powder with a purity of over 98% was bought from Sigma–Aldrich (Zwijndrecht, The Netherlands). MTT [3-(4, 5-dimethylthiazol-2-yl)-2, 5-diphenyltetrazolium bromide], FBS (fetal bovine serum), trypsin-EDTA (ethylenediaminetetraacetic acid), penicillin–streptomycin, and DMEM high glucose medium obtained from Sigma–Aldrich Co. (St Louis, MO, USA). DMSO (Dimethyl sulfoxide), was obtained from Merck (Merck Co., USA). Annexin V-FITC/PI kit (APOAF) (Sigma, USA) and cell culture plates (SPL Life Sciences) were also used. Decoy and Scramble ODNs were synthesized by Bioneer Inc. (Daejeon, Korea). SKBR3 cell line (ATCC number: HTB-30) and MDA-MB-468 cell line (ATCC Number: HTB-132) were provided by the Pasteur Institute of Iran (Tehran, Iran).

2.2. Cell Culture Procedure

SKBR3 and MDA-MB-468 breast cancer cell lines were propagated in DMEM high glucose medium supplemented with 10% FBS, 100 unit/mL penicillin, and 100 µg/mL streptomycin and stored at 37 °C in a humidified atmosphere with 5% CO_2 incubator.

2.3. Design and Synthesis of NANOG Decoy and Scramble ODNs

These NANOG decoy (DEC) and scrambled (SCR) ODNs (Phosphorothioate (PS) modified 18-mer) were previously designed.[33] Briefly, using the nucleotide sequence of the NANOG transcription factor binding site in the human Sox2 gene promoter,

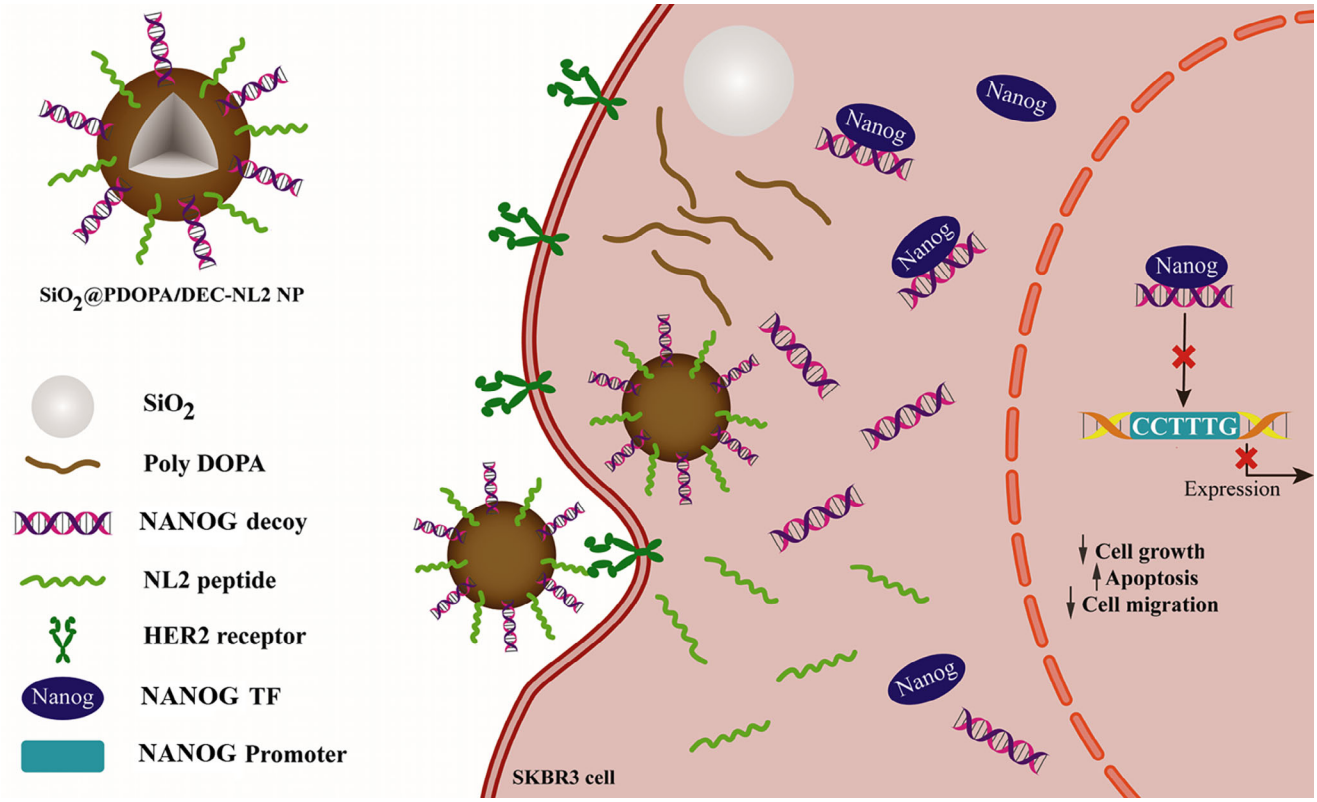

Figure 1. Overview of suppressing the cancerous properties of the SKBR3 breast cancer cells using NL2 peptide-conjugated silica nanoparticles loaded with NANOG decoy oligodeoxynucleotides.

decoy and scramble strands (as mutant negative control) were designed and synthesized (Bioneer Inc, Korea). The temperature of 90 °C for 10 min was applied to the TE solution containing the synthesized sense and antisense strands and allowed to cool slowly to form the double-stranded DEC and SCR. The concentration of double-stranded ODNs was measured using NanoDrop spectrophotometry and stored at 4 °C. The Cy3 fluorescent dye was applied at the 3′ termini to track these ODNs inside the cells. In the sequences of ODNs, the core binding site, PS modifications at 3′ and 5′ ends (for enhanced stability), and three mutations (in scramble ODNs sequences) are shown in boldface, asterisk, and italics/underlined, respectively.

DEC ODN sequences:

F 5′-G*G**CCTTTG**TCATGCTGA*C-3′

R 5′-C*CGGAAACAGTACGACT*G-3′

SCR ODN sequences:

F 5′-G*GC*A*T*GG*GTCATGCTGA*C-3′

R 5′-C*CGTACCCAGTACGACT*G-3′

2.4. Synthesis of Polymeric Core-Shell Nanocomposite

2.4.1. Peptide Synthesis

NL2 peptide with AEGEFIHNRYNRFFYWYGDPAK sequence was selected based on our previous study[32] and was synthesized by solid-phase synthesis method according to fluorene-9-methoxycarbonyl (Fmoc)-polypeptide active ester chemistry by Mimotopes (Mulgrave, Australia). Purification of the synthesized peptides by RP-HPLC method resulted in a 95% purification rate, and the molecular weight and sequence accuracy of these peptides were confirmed by Sciex API100 LC/MS mass spectrometer (Massachusetts, USA).

2.4.2. NANOG Decoy-Loaded Imprinted PDOPA Coating into Silica Nanoparticles

In the synthesis of NANOG decoy-imprinted silica nanoparticles, 0.5 g of nanoparticles were first dispersed in tris buffer (10 mM, pH of 8.5) using a magnetic stirrer for 30 min to achieve a homogenous suspension. Then, 500 mg of PDOPA was added and stirred continuously for 1 h at room temperature to facilitate PDOPA adsorption onto the nanoparticle surface (SiO_2@PDOPA). Subsequently, 500 µL of a 200 nM NANOG decoy solution was introduced, followed by 12 h of stirring at room temperature for imprinting (SiO_2@PDOPA/ODNs). The imprinted nanoparticles were isolated by centrifugation, with the unbound NANOG decoy-containing supernatant discarded. The pellet containing the nanoparticles was then washed three times with nuclease-free deionized water to remove any residual, unbound decoy molecules. Finally, the purified nanoparticles were redispersed in RNase and DNase-free deionized water and stored in a refrigerator for future use.[34]

2.4.3. Synthesis of NL2 Peptide-Functionalized SiO_2@PDOPA/ODNs

To conjugate the peptide onto the polymeric nanocomposite (SiO_2@PDOPA), 2.3 mL of 50 mg/mL *N*-hydroxysuccinimide (NHS) was first added to 5 mL of the nanocomposite solution and stirred rapidly. This was followed by the immediate addition of 1.2 mL of 10 mg/mL 1-ethyl-3-(3-dimethylaminopropyl) carbodiimide (EDC) solution, maintaining the pH between 7.5 and 8 throughout the 2-h stirring period. The suspension was then dialyzed in distilled water for 8 h to remove excess NHS, EDC, and urea byproducts. Subsequently, 1 mL of a 1 mg/mL peptide solution was added to the mixture and stirred for 24 h to facilitate peptide coupling. Finally, the solution underwent dialysis in distilled water for 72 h to remove any unbound peptides. Notably, all steps of the peptide conjugation process were conducted at room temperature.[35,36]

2.5. Nanocomposite Characterization

2.5.1. Characterization of Nanocomposite Morphology, Size, and Zeta Potential

The morphology, surface charge (zeta potential), and hydrodynamic size of the synthesized nanocomposite (SiO_2@PDOPA, SiO_2@PDOPA/ODNs, and SiO_2@PDOPA/ODNs-NL2) were characterized using standard protocols. Scanning Electron Microscopy (SEM) was performed on a ZEISS Gemini SEM 360 (Jena, Germany) to visualize the morphology of the nanocomposite. Dynamic Light Scattering (DLS) using a Zetasizer (Malvern Instruments Ltd, Malvern, United Kingdom) was employed to determine the hydrodynamic size, particle size distribution, and zeta potential of the nanocomposite in suspension.[36,37]

2.5.2. Fourier Transform Infrared (FT-IR) and Ultraviolet–Visible (UV–vis) Spectroscopy

To elucidate the chemical composition and identify functional groups present on the surface of the nanocomposite, Fourier-Transform Infrared (FT-IR) spectroscopy analysis at a range of 400–4000 cm^{-1} was performed using a Biotage instrument (Bruker). Here, 2 mg of the nanocomposite was thoroughly mixed with 200 mg of potassium bromide (KBr) powder. This mixture was then pressed into a compact pellet under a pressure of 12 tons.[37] FT-IR spectroscopy is a nondestructive technique that relies on the absorption of specific infrared radiation by different functional groups in a molecule. This creates a unique "fingerprint" spectrum for each material. By analyzing the obtained FT-IR data, researchers can identify the chemical interactions present between the silica nanoparticles (SiO_2), polydopamine (PDOPA), and the oligonucleotides (ODNs) within the nanocomposite.

The optical properties of SiO_2, SiO_2@PDOPA, and SiO_2@PDOPA/ODNs-NL2 samples were investigated using UV–visible spectroscopy (Shimadzu UV-160 Spectrophotometer, Japan).

2.5.3. NANOG Decoy ODNs Loading and Release from Nanocomposites

The loading efficiency (LE%) of decoy oligonucleotides (ODNs) within the nanocomposites was determined using a centrifugation method.[38] Briefly, the prepared nanocomposites were dispersed in phosphate buffer (pH of 7.4) and centrifuged at 4000 rpm for 30 min to isolate free ODNs. This centrifugation step was repeated at least three times to ensure complete separation of all unbound ODNs from the nanocomposite carrier system. The concentration of the unloaded ODNs in the supernatant was then quantified using a NanoDrop spectrophotometer (Wilmington, USA) at a wavelength of 280 nm.[39] Finally, the LE% of the decoy ODNs was calculated using the following equation:

$$\text{Loading efficiency (LE)} = \frac{\text{Weight of the total decoy ODN} - \text{Weight of free decoy ODN}}{\text{Weight of the nanocomposite}} \times 100$$

The release profile of ODNs (presumably referring to decoy oligonucleotides) from the polymeric nanocomposites was investigated using a NanoDrop spectrophotometer method. Briefly, the nanocomposites were dissolved in a variety of pH buffers, including pH of 7.4 (which mimics physiologic fluid) and pH of 5.8 (which mimics the acidic environment of cancer cell gaps) at 37 °C and subjected to shaking at 150 rpm. At predetermined time points (0, 3, 6, 9, 12, and 24 h), aliquots of the supernatant were collected. The optical density (OD) of these samples was then measured at 280 nm using a Nanodrop spectrophotometer. The concentration of released NANOG decoy ODNs was determined by comparing the OD values to a pre-established standard curve. Finally, a graph was plotted to illustrate the release profile of the ODNs over time.

2.6. Nanocomposite Cellular Uptake Assay

HER2 positive SKBR3 cells (5×10^4 cells/well) and HER2 negative MDA-MB-468 cells (6×10^4cells/well) were seeded in a 12-well plate with 500 µL complete medium and were allowed to grow overnight at 37 °C in 5% CO_2. The SKBR3 cell groups were treated with 500 µL of optimum medium containing SiO_2@PDOPA-NL2 nanocomposites as a negative control group and SiO_2@PDOPA/Labeled ODNs-NL2 nanocomposites (12.5, 25, 50, 100 nM based on labeled ODNs) as a positive control. The MDA-MB-468 cell group was treated with 500 µL of optimum medium containing 100 nM of SiO_2@PDOPA/Labeled ODNs-NL2 nanocomposites. After 24 h, cells were centrifuged at 1200 rpm for 5 min after trypsinization and then resuspended in 500 µL of PBS. Finally, for the cell uptake rate analysis flowcytometry (BD Biosciences, San Jose, CA) and FlowJo v7 software (Tree Star, Ashland, OR) were used.[40]

2.7. Cytotoxicity Assay

HER2 positive SKBR3 cells (1×10^4 cells/well) and HER2 negative MDA-MB-468 cells (1.2×10^4 cells/well) were seeded in a 96-well plate with 200 µL complete medium and were allowed to grow overnight at 37 °C in 5% CO_2. The cell groups were treated with SiO_2@PDOPA-NL2, SiO_2@PDOPA/SCR-NL2, and SiO_2@PDOPA/DEC-NL2 nanocomposites with 12.5, 25, 50, and 100 nM concentrations (based on ODN concentration) for 24 h. Following, 20 µL/well MTT solution (5 mg/mL) was added to the wells and incubated at 37 °C for 4 h. Then, DMSO with a concentration of 100 µL/well was added and the plate was shaken for 10 min. Finally, using an ELISA Reader, the absorbance values at the wavelength of 570/630 nm were detected.[40]

2.8. Apoptosis Assay

HER2 positive SKBR3 cells (5×10^4 cells/well) and HER2 negative MDA-MB-468 cells (6×10^4 cells/well) were seeded in a 12-well plate with 500 µL complete medium and were allowed to grow overnight at 37 °C in 5% CO_2. The cell groups were treated with 50 nM (based on ODN concentration) of SiO_2@PDOPA-NL2, SiO_2@PDOPA/SCR-NL2, and SiO_2@PDOPA/DEC-NL2 nanocomposites for 24 h. Following, the treated cells were stained with Annexin V-FITC and PI according to the manufacturer's protocol. The rate of apoptotic cells was subsequently detected by flow cytometry FACSCalibur (BD Biosciences, San Jose, CA) and analyzed by FlowJo software (Tree Star, Ashland, OR).[41]

2.9. Statistical Analysis

Each assay was performed in triplicate, and data analysis was conducted using GraphPad Prism 8.0 software. Data are presented as mean ± SEM. Statistical significance was determined by one-way and two-way analysis of variance for multiple (>2) groups. *$p < 0.05$, **$p < 0.01$, ***$p < 0.001$, and ****$p < 0.0001$.

3. Results

Description of the synthesized nanoparticles and their corresponding abbreviations used throughout the study (Table 1).

Table 1. Nomenclature and abbreviations of synthesized nanoparticles.

Polydopamine	PDOPA
Silica nanoparticles	SiO_2NPs
Polydopamine-coated Silica nanoparticles	SiO_2@PDOPA
Polydopamine-coated Silica nanoparticles loaded with decoy/scramble ODNs	SiO_2@PDOPA/ODNs
Polydopamine-coated Silica nanoparticles loaded with decoy/scramble ODNs and conjugated with NL2	SiO_2@PDOPA/ODNs-NL2
Polydopamine-coated Silica nanoparticles loaded with Cy3-labeled ODNs and conjugated with NL2	SiO_2@PDOPA/Labeled ODNs-NL2
Polydopamine-coated Silica nanoparticles loaded with NANOG decoy ODNs and conjugated with NL2	SiO_2@PDOPA/DEC-NL2
Polydopamine-coated Silica nanoparticles loaded with NANOG scramble ODNs and conjugated with NL2	SiO_2@PDOPA/SCR-NL2

3.1. Hydrodynamic Size, Surface Charge, and Morphology of Nanocomposites

Dynamic light scattering (DLS) provided insights into the hydrodynamic diameter and zeta potential of the nanocomposites (Figure 2a,b). The average hydrodynamic diameter ranged from 168.32 ± 0.98 nm to 207.31 ± 0.61 nm (mean ± SD) across different formulations, while the zeta potential varied from − 17.75 ± 0.19 mV to − 30.53 ± 0.59 mV (mean ± SD). Additionally, all nanocomposite formulations exhibited a polydispersity index (PDI) below 0.4, indicating a relatively narrow size distribution.

Further characterization using SEM revealed a spherical and uniform morphology for the SiO_2@PDOPA/ODNs-NL2 nanocomposites (Figure 3a). The average size, determined to be 61.03 ± 36.73 nm (mean ± SD), confirms their nanoscale range (Figure 3b), a characteristic size for many nanotechnological applications.

3.2. FTIR Characterization of Nanocomposite

Fourier-transform infrared (FT-IR) spectroscopy was employed to analyze the chemical functionalities present in the synthesized materials. Figure 4a displays the FT-IR spectra of SiO_2@PDOPA (black line), free NL2 (blue line), and SiO_2@PDOPA/ODNs (turquoise line) samples. The spectrum of SiO_2@PDOPA exhibits characteristic peaks at around 3400 cm^{-1} corresponding to O—H stretching vibrations (broad), 1600 cm^{-1} indicative of N—H bending vibrations, 1100 cm^{-1} signifying Si—O—Si stretching vibrations, and 2850 cm^{-1} corresponding to C—H stretching vibrations. These peaks confirm the successful incorporation of both silica and polydopamine within the composite material. The free NL2 spectrum is characterized by a broad peak at 3400 cm^{-1} signifying N—H stretching vibrations. Additionally, a peak at 1650 cm^{-1} suggests C═O stretching vibrations associated with the amide I band. The peak around 1550 cm^{-1} is the amide II band, which is due to the N—H bending vibration and C—N stretching vibration. The spectral analysis of SiO_2@PDOPA/NL2 reveals a composite profile incorporating characteristic peaks from both SiO_2@PDOPA and unbound NL2. Notably, amide I

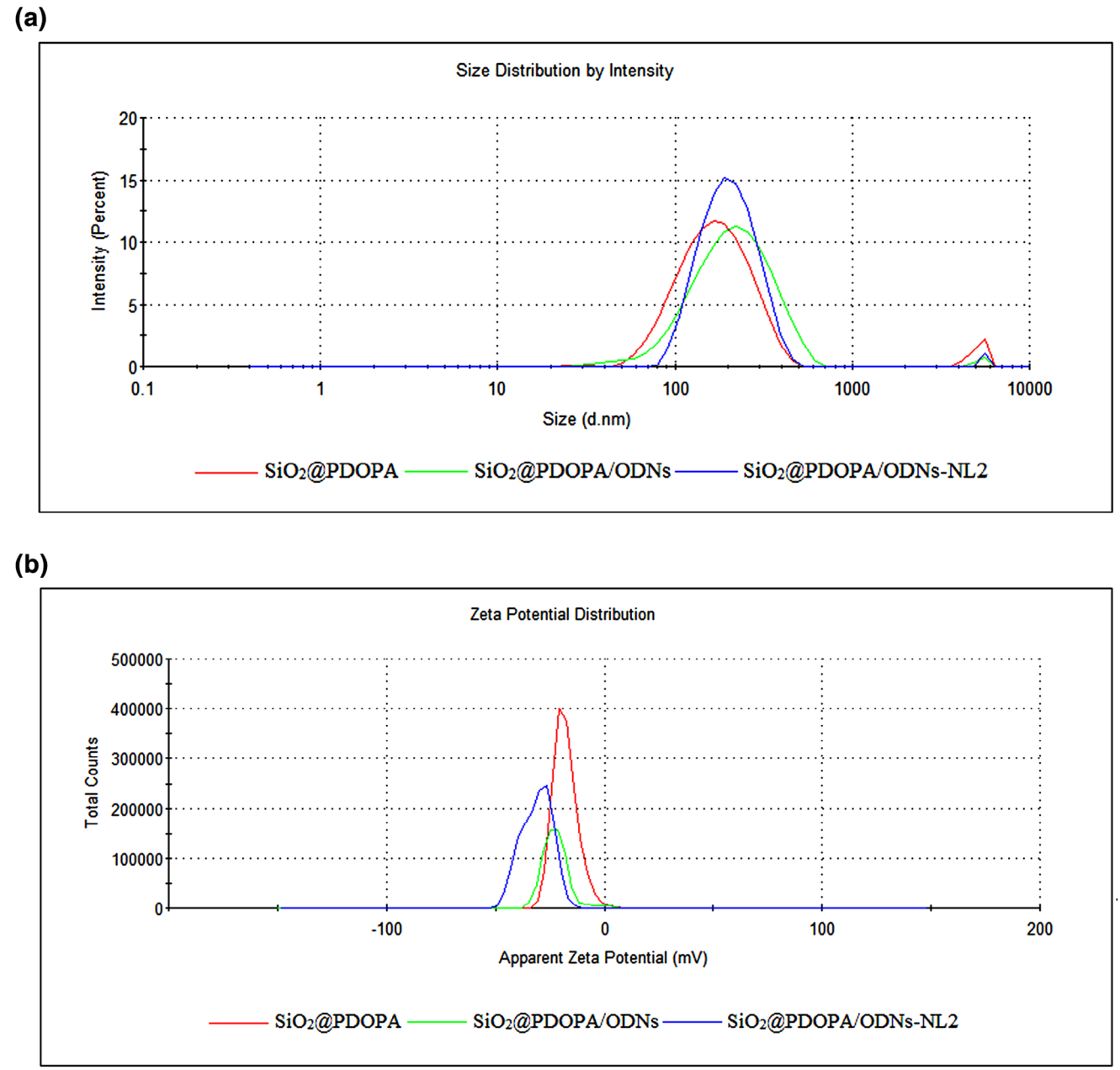

Figure 2. Size and surface charge of nanocomposites analysis by DLS under optimal conditions. (a) Hydrodynamic diameter average size (nm) of synthesized nanocomposites. (b) Zeta-potential average (mV) of synthesized nanocomposites. The analysis was performed under the following conditions: samples were diluted with distilled water to achieve an absorbance of approximately 0.09 at 633 nm, ensuring minimal interference from scattering or aggregation. Measurements were conducted at room temperature (approximately 25 °C) and assumed a refractive index of 1.33, consistent with aqueous environments.

and II vibrational bands provide strong evidence for the successful immobilization of NL2 onto the SiO_2@PDOPA substrate. Moreover, a subtle attenuation in the intensity of PDOPA-associated spectral features is observed when compared to the pristine SiO_2@PDOPA spectrum. This phenomenon suggests a partial occlusion of the PDOPA surface by the adsorbed NL2 molecules, indicating effective surface functionalization. These spectroscopic observations collectively corroborate the efficacious integration of NL2 onto the SiO_2@PDOPA nanocomposite, demonstrating the successful synthesis of the desired SiO_2@PDOPA/NL2 construct.

Figure 4b shows the free ODNs spectrum (green line) that is characterized by a broad peak at 3400 cm^{-1} signifying O—H stretching vibrations. Additionally, a peak at 1700 cm^{-1} suggests C═O stretching vibrations associated with the phosphate backbone of the ODNs. Peaks observed in the range of 1200–1000 cm^{-1} are indicative of P═O and P—O—C stretching vibrations, typical of the phosphate groups present in the ODNs. Spectroscopic analysis of the SiO_2@PDOPA/ODNs composite reveals a complex spectral profile that integrates characteristic features of both SiO_2@PDOPA and unbound ODNs. The presence of distinct amide I and II vibrational bands provides com-

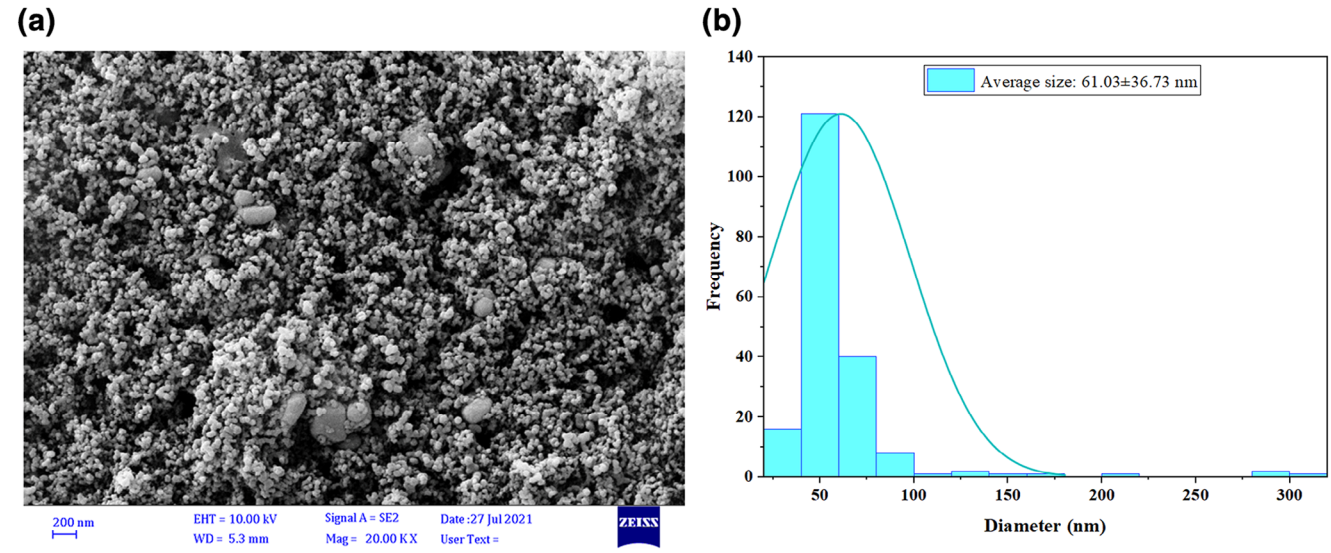

Figure 3. (a) SEM image of SiO_2@PDOPA/ODNs-NL2 nanocomposites showing spherical and uniform morphology. (b) Histogram depicting the size distribution of SiO_2@PDOPA/ODNs-NL2 nanocomposites derived from SEM analysis.

pelling evidence for the successful tethering of ODNs to the SiO_2@PDOPA substrate. Furthermore, a subtle attenuation in the intensity of PDOPA-associated spectral signatures is observed when compared to the spectrum of pristine SiO_2@PDOPA. This phenomenon suggests a partial occlusion of the PDOPA surface by the immobilized ODN molecules, indicative of effective surface functionalization. These spectroscopic observations collectively corroborate the efficacious integration of ODNs onto the SiO2@PDOPA nanocomposite, demonstrating the successful synthesis of the desired SiO2@PDOPA/ODNs construct.

As can be seen in Figure 4c, the spectrum of the SiO_2@PDOPA/ODNs-NL2 nanocomposite displays a combination of peaks from all individual components. The broad peak at 3400 cm^{-1} signifies the presence of both O—H and N—H stretching vibrations. Peaks observed at 2920 cm^{-1} and 2850 cm^{-1} suggest C—H stretching vibrations, potentially arising from aliphatic chains within both PDOPA and NL2. The peak at 1700 cm^{-1} corresponds to C═O stretching vibrations from the ODNs. Additionally, peaks at 1600 cm^{-1} and 1500 cm^{-1} indicate the presence of amide I and amide II bands associated with the NL2 peptide. Finally, the peak at 1100 cm^{-1} represents overlapping contributions from Si—O—Si stretching vibrations in the silica and P═O stretching vibrations from the ODNs.

The presence of these characteristic peaks from all individual components and the observed peak shifts/overlaps suggests successful functionalization of the silica nanoparticles with polydopamine, ODNs, and the NL2 peptide, potentially indicating interactions between these components within the final nanocomposite.

3.3. UV–vis Characterization of Nanocomposite

The UV-vis spectral analysis, as depicted in Figure 5a, reveals distinct absorption profiles for each material (SiO_2, SiO_2@PDOPA, and SiO_2@PDOPA/ODNs-NL2 nanocomposites). The SiO_2 nanoparticles exhibit a characteristic absorption maximum at approximately 290 nm, consistent with the electronic transitions within the silica matrix. Upon functionalization with polydopamine (PDOPA), the resulting SiO_2@PDOPA nanocomposite demonstrates a broad absorption band in the UV region, attributable to the π–π^* electronic transitions of the aromatic moieties present in the PDOPA structure. The subsequent conjugation of oligonucleotides (ODNs-NL2) to form SiO_2@PDOPA/ODNs-NL2 yields a spectral profile that closely resembles that of SiO_2@PDOPA, with a subtle reduction in absorbance intensity observed in the UV region. This spectral similarity suggests that the immobilization of ODNs-NL2 onto the SiO_2@PDOPA surface does not induce significant perturbations in the overall optical properties of the nanocomposite. The preservation of the spectral features indicates that the electronic structure of the PDOPA coating remains largely unaffected by the ODN conjugation process.

3.4. Loading Efficiency of ODNs in SiO_2@PDOPA/ODNs-NL2 Nanocomposite and Release Behavior Assay

The amount of ODNs loading to SiO_2@PDOPA/ODNs-NL2 nanocomposites (with an initial concentration of 50 nM) was determined using a NanoDrop spectrophotometer, and it was calculated as 32.33 ± 5.18 nM by several measurements. As can be seen in Figure 5b, shows the release rate of ODNs at pH = 7.4 for SiO_2@PDOPA/ODNs-NL2. The peak release of the ODNs is within 72 h and the maximum release rate at pH of 7.4 and pH of 5.8 were approximately 69.36 ± 4.03% and 82.73 ± 3.82%, respectively.

3.5. Nanocomposites Loaded with Cy3-labeled ODNs Showed High Uptake in SKBR3 Cells

As shown in Figure 6, the cellular uptake rate was measured after treatment of SiO2@PDOPA/Labeled ODNs-NL2 nanocom-

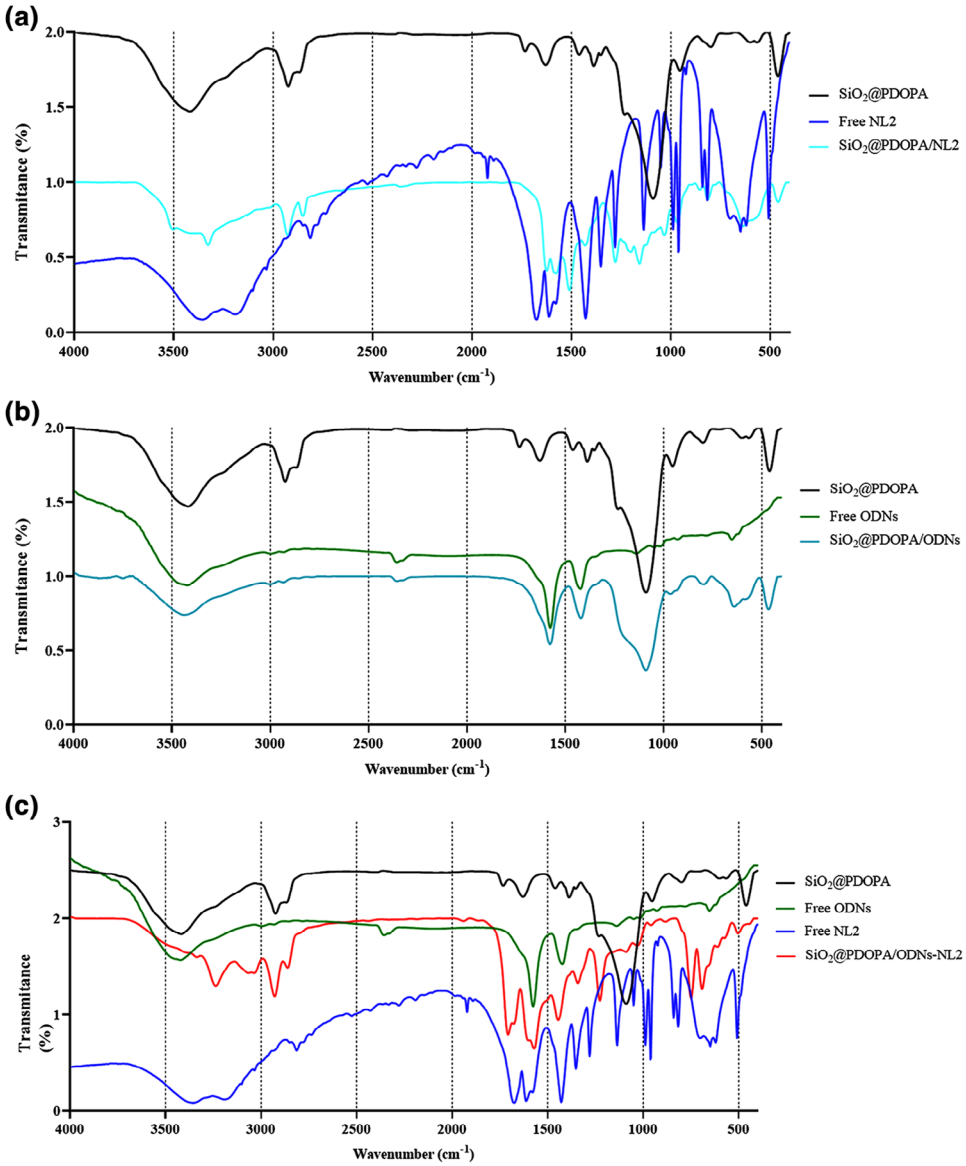

Figure 4. The FTIR spectrum (a-c) SiO_2@PDOPA, free ODNs, free NL2, and SiO_2@PDOPA/ODNs-NL2 nanocomposite showed the successful synthesis of this formulation.

posite by increasing concentrations (12.5, 25, 50, and 100 nM) on SKBR3 cell line and 100 nM concentration on MDA-MB-468 cell line. The amount of cellular uptake rose considerably from 28% to 99% between 12.5 and 100 nM. Around 28% of NPs absorbed by cells in 12.5 nM. There was a more than twofold increase in the amount of cellular absorption between 12.5 nM and 25 nM (64.6%). The percentage for the 50 nM rose significantly to 99% but it remained steady in concentration of 100 nM. It is evident from the bar chart that in all concentrations, the percentage of cellular uptake is significant ($p < 0.0001$) in comparison with ctrl and negative control but there is no change between 50 and 100 nM. The amount of cellular absorption of SiO_2@PDOPA/Labeled ODNs-NL2 nanocomposite with a concentration of 100 nm in the HER2 negative cell line (MDA-MB-468) was lower than the HER2 positive cell line (SKBR3).

3.6. NANOG Decoys-Loaded Nanocomposites Induce Cytotoxicity in SKBR3 Cells

The cytotoxic effects of SiO_2@PDOPA-NL2, SiO_2@PDOPA/DEC-NL2, and SiO_2@PDOPA/SCR-NL2 (12.5–100 nM) on SKBR3 and MDA-MB-468 cancer cells were investigated by MTT assay. Figure 7a shows increasing cytotoxicity in the SiO_2@PDOPA/DEC-NL2 treated SKBR3 groups compared with the control after 24 h. This increase was in a dose-dependent manner. The level of toxicity was lower in the groups treated with SiO_2@PDOPA-NL2 and SiO_2@PDOPA/SCR-NL2 compared to the control. In all treated groups, the maximum rise in cytotoxicity occurred in cells treated with 100 nM. However, this rate of cytotoxicity by SiO_2@PDOPA/DEC-NL2 was significantly higher than the other formulations. In addition, there was a significant difference in terms of toxicity between SiO_2@PDOPA/DEC-NL2 and

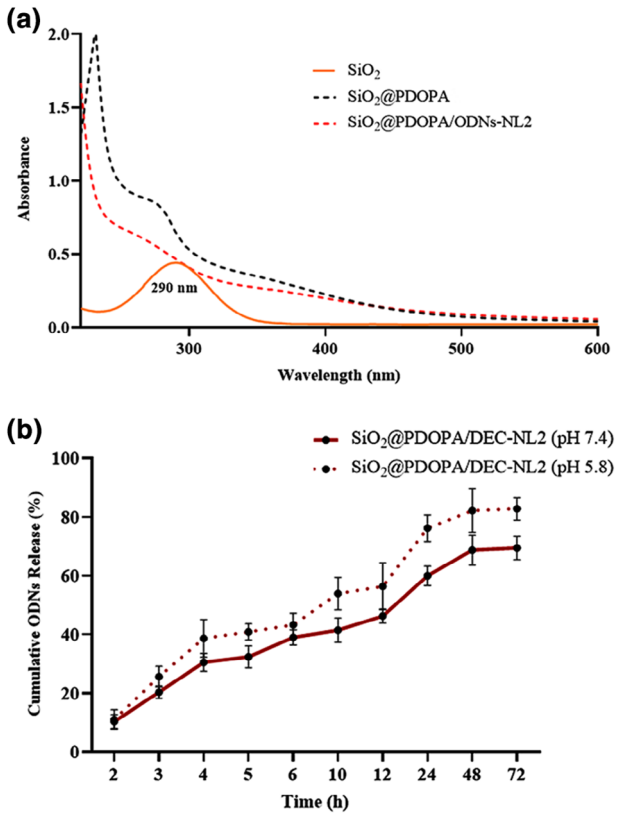

Figure 5. (a) UV–vis absorption spectrum of SiO_2, SiO_2@PDOPA, and SiO_2@PDOPA/ODNs-NL2. (b) In vitro drug-release profiles of ODNs from SiO_2@PDOPA/ODNs-NL2 nanocomposites in both pH (7.4 and 5.8).

SiO_2@PDOPA/SCR-NL2 which indicates the specific function of decoy ODNs on inducing cytotoxicity. As shown in Figure 7c, the toxicity level of these nanocomposites in the MDA-MB-468 cell line is lower than in the SKBR3 cell line.

The obtained results on SKBR3 cells showed that the IC50 value for the SiO_2@PDOPA/DEC-NL2 treated group is 49.35 ± 5.74 nM (Figure 7b). In the MDA-MB-468 cell line, IC50 was not achieved at all concentrations used (Figure 7d).

3.7. NANOG Decoys-Loaded Nanocomposites Increase Apoptosis Rate in SKBR3 Cells

Figure 8a shows the amount of apoptosis (early and late) induction in SKBR3 cells treated with SiO_2@PDOPA-NL2, SiO_2@PDOPA/DEC-NL2, and SiO_2@PDOPA/SCR-NL2 at a concentration of 50 nM, 24 h posttreatment. There was a significant increase in apoptosis rate in SiO_2@PDOPA/DEC-NL2 and SiO_2@PDOPA/SCR-NL2 treated groups as compared to the control (untreated). SiO_2@PDOPA-NL2 had no significant effect on increasing the amounts of apoptotic cells. The apoptosis rate was higher in the cell group treated with SiO_2@PDOPA/DEC-NL2 compared with SiO_2@PDOPA/SCR-NL2. This result may indicate that DEC ODNs have an important role in NANOG transcription factor knockdown and inducing cell apoptosis. In MDA-MB-468 cell groups treated with different groups of nanocomposites, the rate of apoptosis was lower than that of SKBR3 groups (Figure 8b).

4. Discussion

This study presents a novel approach to targeted cancer therapy by combining cutting-edge concepts in nanotechnology and molecular biology. The significance of this research lies in

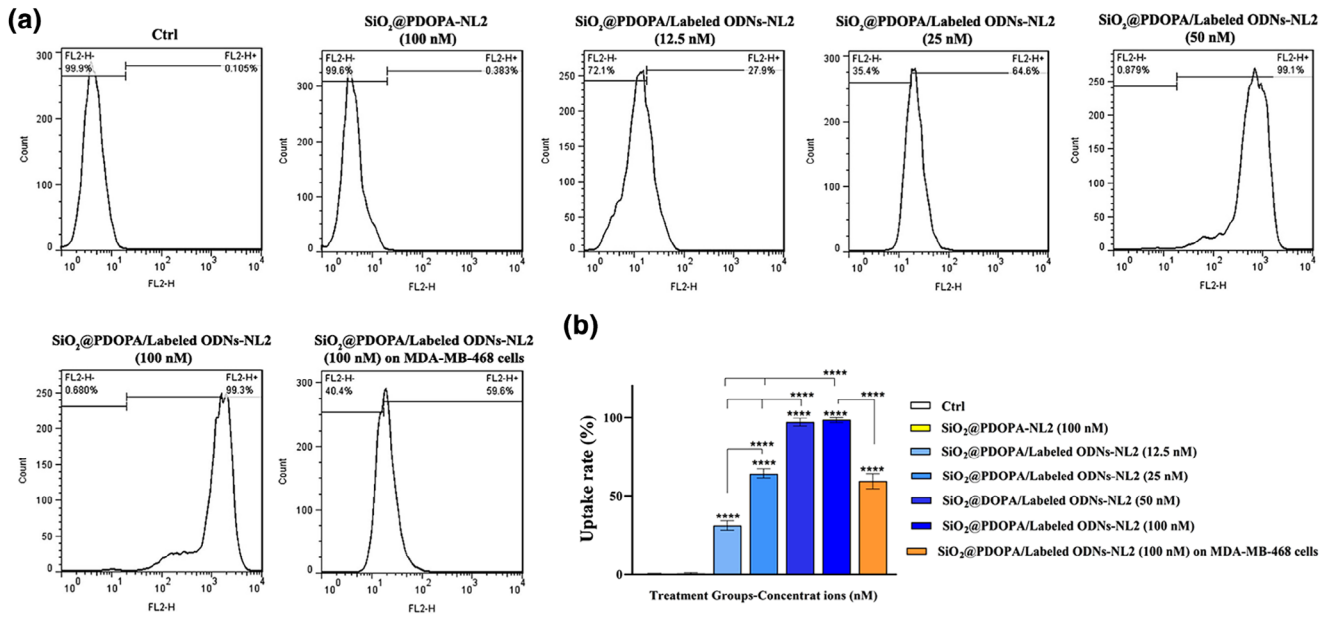

Figure 6. (a) Cellular uptake rate after treatment of SiO_2@PDOPA/Labeled ODNs-NL2 nanocomposite by increasing concentrations (12.5, 25, 50, and 100 nM) on SKBR3 cell line and 100 nM concentration on MDA-MB-468 cell line. (b) The column graph shows the uptake rate in cell-treated groups. Values with **** $p < 0.0001$ were regarded as statistically meaningful.

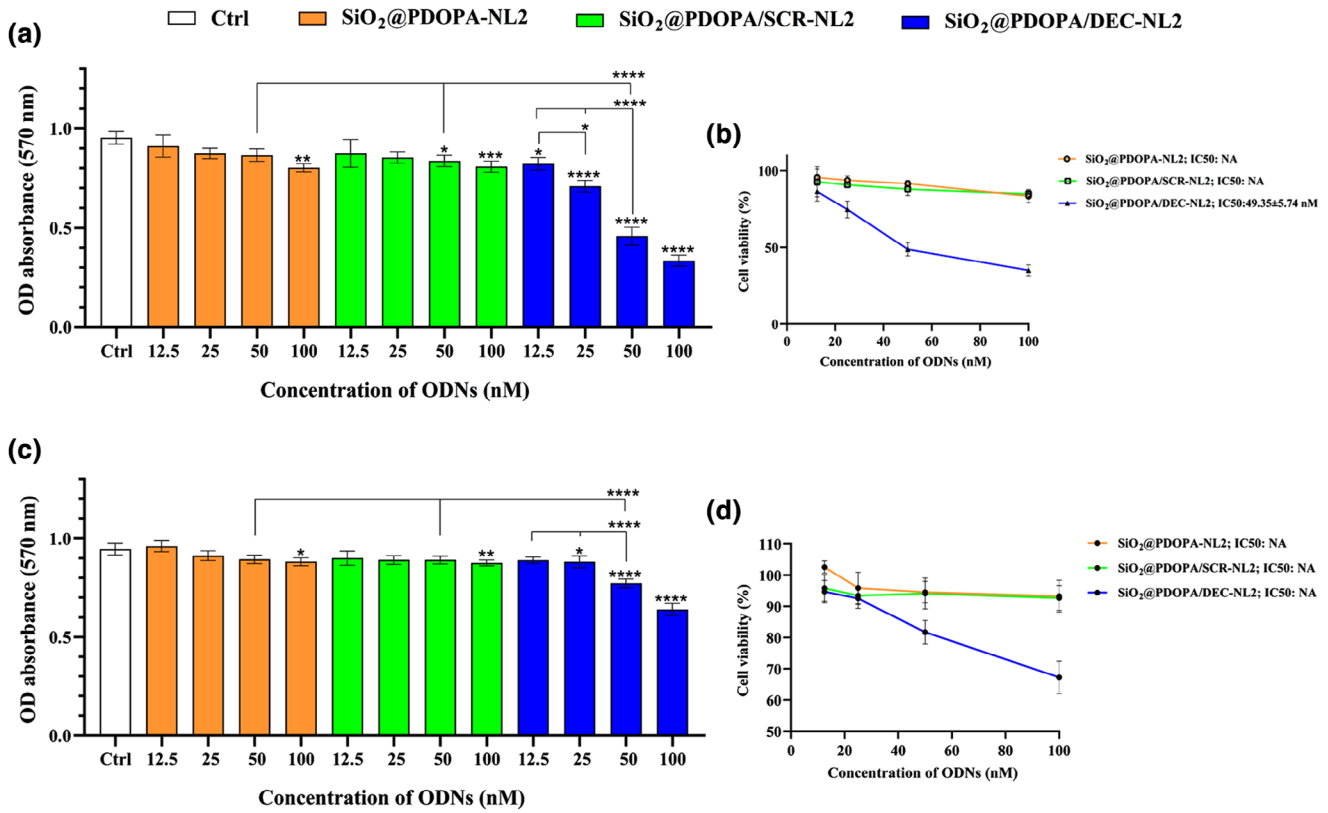

Figure 7. The cytotoxicity and IC50 evaluation of SiO_2@PDOPA-NL2, SiO_2@PDOPA/DEC-NL2, and SiO_2@PDOPA/SCR-NL2 on (a,b) SKBR3 cells and (c,d) MDA-MB-468 cells 24 h after treatment. There was an increase in the cytotoxicity of SiO_2@PDOPA/DEC-NL2 with increasing concentration. This increase in cytotoxicity level in the SKBR3 cell line was higher than in the MDA-MB-468 cell line (*$p < 0.05$, **$p < 0.01$, ***$p < 0.001$, ****$p < 0.0001$, and n = 4).

its potential to overcome the limitations of conventional cancer treatments, particularly the non-specific nature of chemotherapy and radiotherapy, which often result in severe side effects.[42] The novelty of this study is multifaceted, featuring a targeted nanoparticle delivery system using silica nanoparticles conjugated with NL2 peptide, which offers a highly specific mechanism for targeting HER2-positive breast cancer cells. This precision is further enhanced by the use of NANOG decoy oligodeoxynucleotides as the therapeutic payload, addressing a fundamental aspect of cancer biology by targeting a key transcription factor involved in cancer stem cell maintenance and tumor progression.[43] The combination of HER2-targeted nanoparticles with NANOG-specific decoy ODNs creates a dual-targeting system, ensuring selective delivery to HER2-positive cells while specifically inhibiting a crucial transcription factor. This advanced gene regulation approach represents a shift toward more precise molecular interventions in cancer therapy, potentially reducing side effects associated with conventional treatments.[44,45] The significance of this research extends beyond its immediate application in HER2-positive breast cancer, providing a proof-of-concept for a highly adaptable platform that could be modified for other cancer types or molecular targets. Aligning with the growing trend toward personalized medicine in oncology, this study offers a more tailored and potentially more effective treatment strategy, representing a significant advancement in targeted cancer therapy with broader implications for the field of oncology.[46]

In this study, we developed a novel targeted nanocomposite system for the delivery of NANOG decoy oligodeoxynucleotides (ODNs) to HER2-positive SKBR3 and HER2-negative MDA-MB-468 breast cancer cell lines. The innovation lies in the use of NL2 peptide (AEGEFIHNRYNRFFYWYGDPAK), which has a high affinity for the HER2 receptor, to enhance the selectivity of our nanocomposites toward HER2-overexpressing SKBR3 cells.[47] Our comprehensive characterization of the SiO2@PDOPA/DEC-NL2 nanocomposite revealed favorable properties for targeted delivery, including nanometric size (66–307 nm depending on the measurement technique), spherical morphology, and appropriate surface chemistry as confirmed by FTIR spectroscopy.

The difference in nanoparticle size measurements between DLS and SEM stems from the unique principles and conditions of each technique. DLS determines the hydrodynamic diameter of nanoparticles in a liquid medium, factoring in not just the core size but also any surrounding layers, such as adsorbed molecules, surfactants, or hydration shells. This often results in larger reported sizes, particularly for particles with significant surface modifications or in high-ionic-strength solutions. In contrast, SEM provides direct imaging of nanoparticles in a dry state, measuring only the physical dimensions of the particle core without considering surrounding layers. While SEM offers high-resolution details of particle shape and size, it may not fully capture how the particles behave in a liquid environment.

Silica nanoparticles (SNPs) are highly valued for their versatility and potential applications in nanomedicine, material

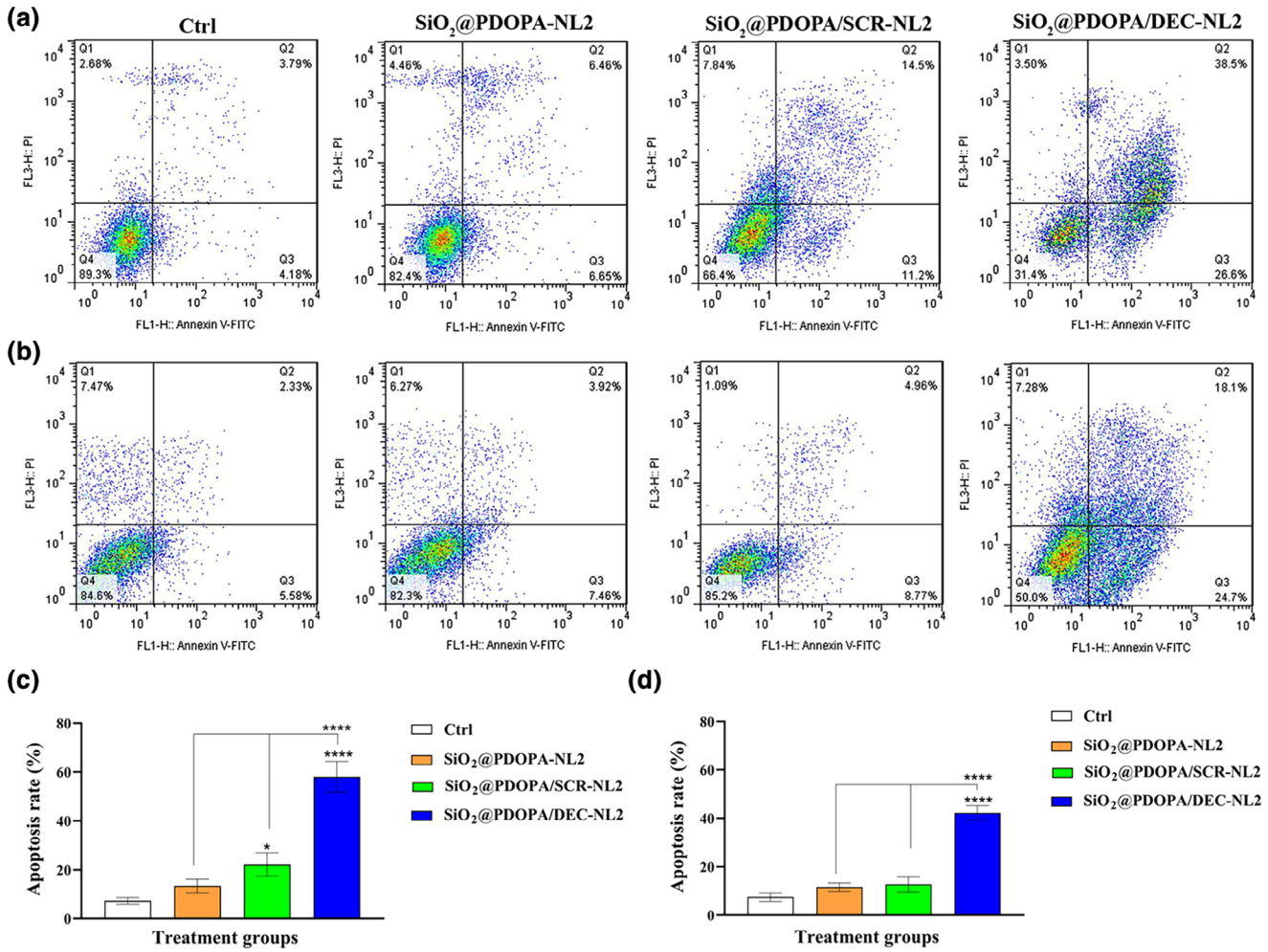

Figure 8. (a,c) The rate of cell apoptosis increased in SKBR3 cells treated with SiO_2@PDOPA/DEC-NL2 (concentration of 50 nM) at 24 h posttreatment. (b,d) The amount of apoptosis in the MDA-MB-468 cell line was lower than in the SKBR3 cell line. One-way ANOVA was used for analysis. *$p < 0.05$ and ****$p < 0.0001$.

sciences, and environmental technology. However, their stability depends on several factors, including particle size, surface modifications, and surrounding environmental conditions. In aqueous solutions, SNPs may experience colloidal instability due to aggregation, primarily driven by van der Waals forces. This effect can be counteracted by electrostatic repulsion. Surface modifications, such as functional group additions or specialized coatings, can further enhance stability by preventing aggregation and improving dispersibility.[48]

The pH and ionic strength of the surrounding medium are crucial factors in determining SNP stability. Acidic or highly saline conditions can destabilize SNP dispersions, promoting aggregation, while alkaline environments and low ionic strength generally enhance stability.[49] Additionally, the extent of silanol group condensation on the nanoparticle surface influences their dissolution rate, with more condensed structures offering greater stability.[50]

Understanding these factors is essential for designing SNPs suited to specific applications, such as drug delivery or imaging, where stability in biological fluids is critical. Ongoing advancements in surface engineering and the development of stabilizing agents are continually enhancing the performance and versatility of SNPs across various fields.

The FT-IR spectroscopy analysis yielded significant insights into the chemical functionalities inherent in the synthesized nanocomposite materials, namely SiO_2@PDOPA, free NL2, SiO_2@PDOPA/ODNs, and the integrated SiO_2@PDOPA/ODNs-NL2. The FT-IR spectra unveiled distinct peaks that correspond to various functional groups, thereby confirming the successful synthesis and functionalization of the nanocomposites. The FT-IR spectrum of SiO_2@PDOPA revealed characteristic peaks at approximately 3400 cm^{-1} (O—H stretching vibrations), 1600 cm^{-1} (N—H bending vibrations), 1100 cm^{-1} (Si—O—Si stretching vibrations), and 2850 cm^{-1} (C—H stretching vibrations). These spectral features are consistent with findings from prior research that has documented similar spectral characteristics for silica-polydopamine composites.[51] The successful integration of silica and polydopamine within the composite material is substantiated by these spectral signatures, indicating effective synthesis. The spectrum associated with free NL2 illustrated a broad peak at 3400 cm^{-1} (N—H stretching vibrations) alongside a peak at 1650 cm^{-1} (C═O stretching vibrations linked to the

amide I band), as well as a peak at 1550 cm^{-1} (amide II band). These observations are in concordance with the recognized vibrational modes of peptides and proteins. The spectrum of the SiO_2@PDOPA/NL2 composite exhibited a composite profile that incorporates characteristic peaks from both SiO_2@PDOPA and unattached NL2, particularly the amide I and II bands. The reduction in the intensity of PDOPA-associated spectral features suggests a degree of occlusion of the PDOPA surface by the adsorbed NL2 molecules, indicative of successful surface functionalization. The FT-IR spectrum of free ODNs was characterized by a broad peak at 3400 cm^{-1} (O—H stretching vibrations) and a peak at 1700 cm^{-1} (C═O stretching vibrations associated with the phosphate backbone). Peaks observed within the 1200–1000 cm^{-1} range were indicative of P═O and P—O—C stretching vibrations, which are typical of phosphate groups in ODNs (Chen et al., 2020). The SiO_2@PDOPA/ODNs composite exhibited a complex spectral profile that integrates features from both SiO_2@PDOPA and unbound ODNs. The presence of amide I and II vibrational bands, along with the attenuation of PDOPA-associated spectral signatures, suggests effective surface functionalization by ODNs. The spectrum of the SiO_2@PDOPA/ODNs-NL2 nanocomposite displayed a combination of peaks from all individual components, encompassing broad peaks at 3400 cm^{-1} (O—H and N—H stretching vibrations), 2920 cm^{-1} and 2850 cm^{-1} (C—H stretching vibrations), and 1700 cm^{-1} (C═O stretching vibrations from ODNs). Peaks at 1600 cm^{-1} and 1500 cm^{-1} indicated the presence of amide I and II bands associated with the NL2 peptide. The peak at 1100 cm^{-1} represented overlapping contributions from Si—O—Si stretching vibrations in silica and P═O stretching vibrations from ODNs.[52,53] These findings imply successful functionalization of the silica nanoparticles with polydopamine, ODNs, and the NL2 peptide, potentially indicating interactions among these components within the final nanocomposite.

The UV–vis spectral examination of the synthesized nanocomposites yields profound insights into the optical characteristics and successful functionalization of the materials. The distinct absorption spectra recorded for SiO_2, SiO_2@PDOPA, and SiO_2@PDOPA/ODNs-NL2 nanocomposites affirm the presence and integration of each constituent within the composites. The UV–vis spectrum of the SiO_2 nanoparticles revealed a distinctive absorption maximum at approximately 290 nm, which corresponds to electronic transitions occurring within the silica matrix. This observation is in concordance with prior investigations that have documented analogous absorption characteristics for silica nanoparticles.[54] The absorption at 290 nm signifies the intrinsic electronic properties of the silica matrix, providing a foundational reference for subsequent functionalization. Following functionalization with polydopamine (PDOPA), the resulting SiO_2@PDOPA nanocomposite exhibited a broad absorption band within the ultraviolet region. This spectral broadening can be attributed to the π–π^* electronic transitions associated with the aromatic moieties inherent in the PDOPA structure. Comparable observations have been documented in the literature, wherein polydopamine coatings on various substrates display characteristic broad UV absorption due to their conjugated aromatic systems.[55] The broad absorption band substantiates the effective coating of the SiO_2 nanoparticles with PDOPA, thereby enhancing their optical properties. The UV–vis spectrum of the SiO_2@PDOPA/ODNs-NL2 nanocomposite closely mirrored that of SiO_2@PDOPA, with a marginal reduction in absorbance intensity noted in the ultraviolet region. This spectral resemblance implies that the immobilization of ODNs-NL2 onto the SiO_2@PDOPA surface does not elicit significant perturbations in the overall optical properties of the nanocomposite. The retention of the spectral characteristics suggests that the electronic structure of the PDOPA coating remains predominantly unaffected by the ODN conjugation process. This observation aligns with other investigations that have indicated minimal alterations in the UV-vis spectra following the functionalization of polydopamine-coated nanoparticles with biomolecules.[56,57]

The cellular uptake of SiO2@PDOPA/Labeled ODNs-NL2 nanocomposite with a concentration of 100 nm was lower in the HER2 negative cell line (MDA-MB-468) in comparison to the HER2 positive cell line (SKBR3). The reason can be the lack of HER2 receptor on the MDA-MB-468 cell line and non-targeting of these cells with the NL2 ligand present on the nanocomposites. The level of cytotoxicity and apoptosis was lower in the MDA-MB-468 cell line compared to the SKBR3 cell line, which could be due to insufficient internalization of nanocomposites in these HER2-negative cells. The significance of our approach is underscored by the critical role of NANOG in cancer progression and treatment resistance. Our results demonstrated that the delivery of NANOG-specific decoy ODNs to SKBR3 cells effectively reduced NANOG expression, leading to increased cytotoxicity in these cancer cells. Notably, the SiO_2@PDOPA/DEC-NL2 nanocomposite showed superior cytotoxic effects on the SKBR3 cell line compared to control nanoparticles, highlighting the specificity and efficacy of our NANOG decoy strategy.[52] These findings align with previous studies that have shown the inhibition of tumor growth, sphere formation, and drug resistance upon NANOG knockdown in various cancer models. Furthermore, our approach potentially interferes with the TGF-β/SMAD signaling pathway, known to regulate cell proliferation, apoptosis, and differentiation. By targeting NANOG, a key transcription factor in cancer stem cell maintenance and tumor progression, our nanocomposite system offers a novel therapeutic strategy that could overcome the limitations of conventional cancer treatments, particularly in addressing treatment resistance and tumor recurrence in HER2-positive breast cancers.[58–60]

The choice of 50 nM for the apoptosis study was guided by cytotoxicity assay and IC50 evaluation, which showed that this concentration effectively reduced cell viability while avoiding excessive toxicity. In our study, we observed significant cellular effects on SKBR3 cells following treatment with SiO2@PDOPA/DEC-NL2 nanocomposites, specifically an increase in apoptosis. These findings align with the established role of NANOG in cancer progression and stem cell maintenance.[61] The impact of NANOG suppression on apoptosis has been well-documented across various cancer types.[61] Similarly, studies in mouse embryonic stem cells have demonstrated that NANOG

silencing increases the proportion of cells in the G0/G1 phase and induces apoptosis, accompanied by elevated caspase-3 activation.[62] Our results extend these findings to HER2-positive breast cancer cells, suggesting that targeted NANOG suppression via decoy ODNs can effectively disrupt the cell cycle and promote apoptosis in cancer stem cells (CSCs). This is particularly significant given the role of CSCs in therapy resistance and tumor recurrence.[63]

Silica-based nanoparticles (SNPs) have gained attention in nanomedicine for their high biocompatibility and customizable surface properties. However, their potential immunogenic effects are an important consideration for clinical use. Research indicates that SNPs can interact with immune cells, such as macrophages and dendritic cells, potentially activating inflammatory pathways.[64] The surface charge, size, and functionalization of SNPs play key roles in shaping immune responses. For example, positively charged SNPs are more likely to trigger cytokine release compared to their neutral or negatively charged counterparts.[65] Additionally, mesoporous silica nanoparticles (MSNs) have demonstrated potential in immunotherapy by serving as carriers for immunomodulatory agents.[66] Oligodeoxynucleotide (ODN) therapeutics, especially those with unmethylated CpG motifs, are powerful immune stimulators. They activate Toll-like receptor 9 (TLR9) on plasmacytoid dendritic cells, triggering the production of pro-inflammatory cytokines and enhancing Th1-type immune responses.[67] However, the immunogenicity of ODNs can vary depending on their sequence and chemical modifications.[68] Integrating ODNs with nanoparticles as delivery platforms has been explored to improve stability and targeted delivery while reducing systemic immune activation.[69] This synergy highlights the importance of optimizing nanoparticle design to balance therapeutic effectiveness with immunogenic safety.

This study demonstrates the effective in vitro performance of our NL2-functionalized silica nanoparticles in delivering NANOG decoy ODNs to their target. However, to fully realize their potential, further in vivo studies are crucial. These studies will aim to assess their therapeutic efficacy, biodistribution, and pharmacokinetics in a biologically relevant model. Moving forward, we aim to conduct animal studies to validate these findings and explore the clinical potential of this promising nanoplatform.

5. Conclusion

In this study, SiO_2@PDOPA/DEC-NL2 nanocomposite with suitable properties was prepared. These synthesized nanocomposites successfully delivered NANOG decoys to the SKBR3 breast cancer cell line by targeting the HER2 receptor. The percentage of cell uptake of NL2-targeted nanocomposite on the SKBR3 cell line was high. The NL2-targeted SiO_2@PDOPA/DEC-NL2 nanocomposite containing NANOG-specific decoys significantly increased cytotoxicity and apoptosis rate in the SKBR3 cells compared to MDA-MB-468 cells. These findings highlight the therapeutic potential of targeted NANOG inhibition in HER2-positive breast cancer and potentially other NANOG-dependent malignancies. Altogether, the SiO_2@PDOPA/DEC-NL2 nanocomposite has the potential to be used as a drug delivery system in future in vivo studies.

Author Contributions

Roghayeh Ghorbani: Methodology and writing. **Mahmoud Gharbavi**: Review, editing, and final approval. **Behrooz Johari**: Supervision; project administration; conceptualization; writing—original draft, review and editing, and final approval. **Zahra Bigdelou**: Methodology. **Zeinab Pourmansouri**: Methodology. **Niloofar Asadi**: Methodology. **Nazli Aghapur**: Methodology. **Benyamin Keshavarz**: Methodology. **Hamid Madanchi**: Project administration; methodology; conceptualization; software; editing, and final approval.

Acknowledgements

M.G. and R.G. contributed equally to this work and are co-first authors. The authors express their gratitude toward the staff of the Medical Biotechnology Department at Semnan and Zanjan University of Medical Sciences. The present study was supported by Semnan University of Medical Sciences, Semnan, Iran (Grant Number: 3590 and Ethical Code: IR.SEMUMS.REC.1402.211).

Conflict of Interests

The authors declare no conflict of interest.

Data Availability Statement

The data that support the findings of this study are available from the corresponding author upon reasonable request.

Keywords: Breast cancer · Decoy oligodeoxynucleotides · HER2-positive · NL2 peptide · Silica nanoparticles

[1] H. Sung, J. Ferlay, R. L. Siegel, M. Laversanne, I. Soerjomataram, A. Jemal, F. Bray, *Ca-Cancer J. Clin.* **2021**, *71*, 209–249.
[2] M. Arnold, E. Morgan, H. Rumgay, A. Mafra, D. Singh, M. Laversanne, J. Vignat, J. R. Gralow, F. Cardoso, S. Siesling, I. Soerjomataram, *The Breast* **2022**, *66*, 15–23.
[3] H. Takeshima, T Ushijima, *NPJ Prec. Oncol.* **2019**, *3*, 7.
[4] J. H Bushweller, *Nat. Rev. Cancer* **2019**, *19*, 611-624.
[5] G. Grubelnik, E. Boštjančič, A. Pavlič, M. Kos, N Zidar, *Exp. Biol. Med.* **2020**, *245*, 456–464.
[6] X. Lu, S. J. Mazur, T. Lin, E. Appella, Y Xu, *Oncogene* **2014**, *33*, 2655–2664.
[7] T. Nagata, Y. Shimada, S. Sekine, R. Hori, K. Matsui, T. Okumura, S. Sawada, J. Fukuoka, K. Tsukada, *Breast Cancer* **2014**, *21*, 96–101.
[8] C Jeter, *Stem Cells* **2005**, *209*, 993.
[9] Z. Aliyari-Serej, A. Ebrahimi, T. Kazemi, S. Najafi, E. Roshani, M. Ebrahimi-Kalan, B. Baradaran, *Immunopathologia Persa* **2020**, *6*, e21.
[10] S. Winters, C. Martin, D. Murphy, N. K Shokar, *Progress. Molecular Biol. Translational Sci.* **2017**, *151*, 1–32.
[11] S. Palomeras, S. Ruiz-Martínez, T Puig, *Molecules* **2018**, *23*, 2193.

[12] S. Hajighasemlou, M. Alebouyeh, H. Rastegar, M. T. Manzari, M. Mirmoghtadaei, B. Moayedi, M. Ahmadzadeh, F. Parvizpour, B. Johari, M. M. Naeini, M. M. Farajollahi, *Asian Pac. J. Cancer Prev.* **2015**, *16*, 5977–5981.
[13] K. Zhang, P. Li, Y. He, X. Bo, X. Li, D. Li, H. Chen, H. Xu, *Biomaterials* **2016**, *99*, 34–46.
[14] M. Vilalta, M. Rafat, E. E Graves, *Cell. Mol. Life Sci.* **2016**, *73*, 2999–3007.
[15] Z. Zhao, X. Zhang, C.-e. Li, T Chen, *Biomaterials* **2019**, *192*, 579–589.
[16] A. Burguin, C. Diorio, F Durocher, *J. Personal. Med.* **2021**, *11*, 808.
[17] B. Johari, M. Ebrahimi-Rad, F. Maghsood, M. Lotfinia, Z. Saltanatpouri, L. Teimoori-Toolabi, Z. Sharifzadeh, M. Karimipoor, M. Kadivar, Anti-Cancer Agents Med. Chem (Formerly Current Medicinal Chemistry-Anti-Cancer Agents). **2017**, *17*, 1786-95.
[18] H. Nakagami, M. Osako, N. Tomita, R Morishita, *RNA Technologies in Cardiovascular Medicine and Research*, Springer, Berlin, Germany **2008**, pp. 299–309.
[19] M. K. Osako, H. Nakagami, R Morishita, *Nucleic Acid Drugs* **2012**, 49–59.
[20] B. Johari, M Moradi, *Gene Therapy of Cancer, Methods, and Protocols*, Springer, Berlin, Germany **2022**. pp. 207–30.
[21] G. A. H. Kim, J. I. E. Won, Y. Byeon, M. G. Kim, T. I. Wi, J. M. Lee, Y.-Y. Park, J.-W. Lee, T. H. Kang, I. D. Jung, B. C. Shin, H. J. Ahn, Y. J. Lee, A. K. Sood, H. D. Han, Y.-M. Park, *Drug Delivery* **2018**, *25*, 1394–1402.
[22] P. Ratnasamy, D. Srinivas, C. V. V. Satyanarayana, P. Manikandan, R. S. Senthil Kumaran, M. Sachin, V. N. Shetti, *J. Catal.* **2004**, *221*, 455–465.
[23] S. Ribeiro, R. M. Meira, D. M. Correia, C. R. Tubio, C. Ribeiro, C. Baleizão, S. Lanceros-Méndez, *Composites, Part B* **2020**, *185*, 107786.
[24] M. Jaber, J.-F Lambert, *J. Phys. Chem. Lett.* **2010**, *1*, 85–88.
[25] X. Zhang, K. Achazi, D. Steinhilber, F. Kratz, J. Dernedde, R Haag, *J. Controlled Release* **2014**, *174*, 209–216.
[26] M. Shi, J. Zhang, J. Li, Y. Fan, J. Wang, W. Sun, H. Yang, C. Peng, M. Shen, X. Shi, *J. Mater. Chem. B* **2019**, *7*, 368–372.
[27] H. Hashemi-Moghaddam, S. Zavareh, E. M. Gazi, M Jamili, *Mater. Sci. Eng., C* **2018**, *93*, 1036–1043.
[28] P. Busa, R. Koutavarapu, Y Kuthati, *Coatings* **2022**, *12*, 60.
[29] A. Z. Wilczewska, K. Niemirowicz, K. H. Markiewicz, H Car, *Pharmacol. Rep.* **2012**, *64*, 1020–1037.
[30] J. D. Byrne, T. Betancourt, L Brannon-Peppas, *Adv. Drug Delivery Rev.* **2008**, *60*, 1615–1626.
[31] N. Muhamad, T. Plengsuriyakarn, K Na-Bangchang, *Int. J. Nanomed.* **2018**, *13*, 3921–3935.
[32] M. Nazemian, V. Hojati, S. Zavareh, H. Madanchi, H Hashemi-Moghaddam, *Int. J. Pept. Res. Ther.* **2020**, *26*, 259–269.
[33] M. Gharbavi, B. Johari, E. Rismani, N. Mousazadeh, A. H. Taromchi, A Sharafi, *ACS Chem. Neurosci.* **2020**, *11*, 4499–4515.
[34] M. Mirzababaei, K. Larijani, H. Hashemi-Moghaddam, Z. Mirjafary, H Madanchi, *J. Fluoresc.* **2021**, *31*, 279–288.
[35] H. Hashemi-Moghaddam, M. Ebrahimi, B. Johari, H Madanchi, *J. Biomed. Mater. Res., Part B* **2021**, *109*, 1578–1587.
[36] B. Jafari, M. Gharbavi, Y. Baghdadchi, H. K. Manjili, J. Mahmoudi, I. Jafari-Anarkoli, S. Amiri, M. J. Hosseini, *Behavioural Neurology* **2022**, *2022*, 4825472.
[37] M. Gharbavi, B. Johari, R. M. Tabar, A Sharafi, *Appl. Organomet. Chem.* **2024**, *38*, e7327.
[38] R. Ghorbani, M. Gharbavi, B. Keshavarz, H. Madanchi, B Johari, *Mol. Biol. Rep.* **2024**, *51*, 623.
[39] H. Mohammadzade, H. Hashemi-Moghaddam, L. Beikzadeh, A. Ahmadieh-Yazdi, H. Madanchi, P Fallah, *Drug Deliv. Translat. Res.* **2023**, 1–16.
[40] B. Johari, S. Tavangar-Roosta, M. Gharbavi, A. Sharafi, S. Kaboli, H Rezaeejam, *Heliyon* **2024**, *10*, e34096.
[41] M. Rahmati, B. Johari, M. Kadivar, E. Rismani, Y Mortazavi, *J. Cell. Physiol.* **2020**, *235*, 5429–5444.
[42] A. B. Kunnumakkara, P. Diagaradjane, S. Guha, A. Deorukhkar, S. Shentu, B. B. Aggarwal, S. Krishnan, *Clin. Cancer Res.* **2008**, *14*, 2128–2136.
[43] C. K. Nair, D. K. Parida, T Nomura, *J. Radiation Res.* **2001**, *42*, 21–37.
[44] J. F. Hainfeld, F. A. Dilmanian, D. N. Slatkin, H. M Smilowitz, *J. Pharm. Pharmacol.* **2008**, *60*, 977–985.
[45] F. Chen, X. H. Zhang, W. Zhang, Z. C. Lou, L. H. Xie, X. D. Hu, L. peidang, H. Q. Zhang, *Int. J. Nanomed.* **2015**, *10*, 4957.
[46] R. Kanasty, J. R. Dorkin, A. Vegas, D Anderson, *Nat. Mater.* **2013**, *12*, 967–977.
[47] A. Lamprecht, N. Ubrich, H. Yamamoto, U. Schäfer, H. Takeuchi, P. Maincent, Y. Kawashima, C.-M. Lehr, *J. Pharmacol. Exp. Ther.* **2001**, *299*, 775–781.
[48] C. da , A. Schneid, L. J. C. Albuquerque, G. B. Mondo, M. Ceolin, A. S. Picco, M. B Cardoso, *J. Sol–Gel Sci. Technol.* **2022**, *102*, 41–62.
[49] L. Spitzmüller, F. Nitschke, B. Rudolph, J. Berson, T. Schimmel, T Kohl, *J. Nanopart. Res.* **2023**, *25*, 40.
[50] C. O. Metin, L. W. Lake, C. R. Miranda, Q. P Nguyen, *J. Nanopart. Res.* **2011**, *13*, 839–850.
[51] M. Shao, C. Chang, Z. Liu, K. Chen, Y. Zhou, G. Zheng, Z. Huang, H. Xu, P. Xu, B. Lu, *Colloids Surf., B* **2019**, *183*, 110427.
[52] C. Heng, M. Liu, K. Wang, X. Zheng, H. Huang, F. Deng, J. Hui, X. Zhang, Y. Wei, *RSC Adv.* **2015**, *5*, 91308–91314.
[53] T. N. Tran, T. V. A. Pham, M. L. P. Le, T. P. T Nguyen, *Adv. Nat. Sci. Nanosci. Nanotechnol.* **2013**, *4*, 045007.
[54] M. Ramazanov, H. Shirinova, S. Nuriyeva, M. Jafarov, M Hasanova, *J. Thermoplastic Comp. Mater.* **2023**, *36*, 1762–1774.
[55] Y. Liu, K. Ai, L Lu, *Chem. Rev.* **2014**, *114*, 5057–5115.
[56] S. Lu, J. Yu, Y. Cheng, Q. Wang, A. Barras, W. Xu, S. Szunerits, D. Cornu, R. Boukherroub, *Appl. Surf. Sci.* **2017**, *411*, 163–169.
[57] D. Ö. Özgür, *Micropor. Mesopor. Mater.* **2021**, *314*, 110861.
[58] T. Yoshimoto, T. Fujita, M. Kajiya, S. Matsuda, K. Ouhara, H. Shiba, H. Kurihara, *Cytokine* **2015**, *75*, 165–173.
[59] P. Xu, J. Liu, R Derynck, *FEBS Lett.* **2012**, *586*, 1871—1884.
[60] K Miyazono, *Cytokine Growth Factor Rev.* **2000**, *11*, 15–22.
[61] J. Han, F. Zhang, M. Yu, P. Zhao, W. Ji, H. Zhang, B. Wu, Y. Wang, R. Niu, *Cancer Lett.* **2012**, *321*, 80–88.
[62] T. Chen, J. Du, G Lu, *Mol. Biol. Rep.* **2012**, *39*, 1855–1861.
[63] M. K. Y. Siu, E. S. Y. Wong, D. S. H. Kong, H. Y. Chan, L. Jiang, O. G. W. Wong, E. W.-F. Lam, K. K. L. Chan, H. Y. S. Ngan, X.-F. Le, A. N. Cheung, *Oncogene* **2013**, *32*, 3500–3509.
[64] B. Gu, Q. Zhao, Y Ao, *Biomolecules* **2024**, *14*, 1057.
[65] H. Wu, X.-F. Xu, J.-Q. Zhu, M.-D. Wang, C. Li, L. Liang, H. Xing, M.-C. Wu, F. Shen, D.-S. Huang, T. Yang, *Front. Bioeng. Biotechnol.* **2021**, *9*, 695635.
[66] J. Zhang, F. Wang, Z. Sun, J. Ye, H Chu, *J. Nanobiotechnol.* **2025**, *23*, 161.
[67] Z. K. Ballas, A. M. Krieg, T. Warren, W. Rasmussen, H. L. Davis, M. Waldschmidt, G. J. Weiner, *J. Immunol.* **2001**, *167*, 4878–4886.
[68] O. M. Kudriavtseva, A. P. Semakova, N. I. Mikshis, P. Y. u. Popova, V. A. Kozhevnikov, A. V. Stepanov, S. A. Bugorkova, *Appl. Biochem. Microbiol.* **2018**, *54*, 855–862.
[69] M. Li, H. Yao, K. Yi, Y.-H. Lao, D. Shao, Y Tao, *Biomater. Sci.* **2024**, *12*, 2203–2228.

Manuscript received: January 30, 2025